Total photoabsorption cross sections for ^{1}H, ^{2}H, and ^{3}He from 200 to 800 MeV

M. MacCormick,* G. Audit, N. d'Hose, L. Ghedira,† V. Isbert, S. Kerhoas, L. Y. Murphy, G. Tamas, and P. A. Wallace‡
Service de Physique Nucléaire - DAPNIA, Centre d'Etudes de Saclay, 91191 Gif-sur-Yvette, France

S. Altieri,[1,2] A. Braghieri,[1,2] P. Pedroni,[1,§] and T. Pinelli[1,2]
[1]*Istituto Nazionale di Fisica Nucleare, Sezione di Pavia, via Bassi 6, 27100 Pavia, Italy*
[2]*Dipartimento di Fisica Nucleare e Teorica, Università degli Studi di Pavia, via Bassi 6, 27100 Pavia, Italy*

J. Ahrens and R. Beck
Institut für Kernphysik, Universität Mainz, D-55099 Mainz, Germany

J. R. M. Annand, R. A. Crawford, J. D. Kellie, and I. J. D. MacGregor
Department Of Physics and Astronomy, University of Glasgow, United Kingdom

B. Dolbilkin and A. Zabrodin
Institute for Nuclear Research, 7a, Prospect 60 Let Oktyabrya, 117312, Moscow, Russia
(Received 16 February 1995)

The total photoabsorption cross sections for ^{1}H, ^{2}H, and ^{3}He have been measured for incident photon energies ranging from 200 to 800 MeV. The ^{3}He data are the first for this nucleus. By using the large acceptance detector DAPHNE in conjunction with the tagged photon beam facility of the MAMI accelerator in Mainz, cross sections of high precision have been obtained. The results show clearly the changes in the nucleon resonances in going from ^{1}H to ^{3}He. In particular, for the D_{13} region the behavior for ^{3}He is intermediate between that for ^{1}H, ^{2}H, and heavier nuclei. This will provide a strong constraint to the theories that are presently being developed with a view to explaining the apparent ''damping'' of higher resonances in heavy nuclei.

PACS number(s): 25.20.−x, 13.60.Rj, 24.30.Gd

I. INTRODUCTION

The ''universal'' behavior of the total photoabsorption cross section per nucleon ($\sigma_{\rm tot}/A$) in the $\Delta(1232)$ resonance region was well established about 10 years ago (see reviews [1–3]). Compared to the free nucleon, the peak cross section in the resonance for bound nucleons is reduced but the Δ resonance width is increased. Since the integrated total cross section remains roughly constant in all cases, the total photoabsorption strength is conserved.

Recently, experiments carried out by groups at Frascati and Mainz [4–8] have provided measurements of $\sigma_{\rm tot}$ for Li, Be, C, Al, Pb, Sn, and U up to 1.2 GeV. The results of these experiments confirm the trends indicated by the older Yerevan data [9,10]. The higher $D_{13}(1520)$ and $F_{15}(1680)$ resonances that are clearly seen on the proton and deuteron are no longer visible in the heavier nuclei. Furthermore, the total photoabsorption strength per nucleon is reduced. The mechanism behind this apparent ''damping'' is not as yet well understood.

This paper presents the results of a study that was carried out on light nuclei (^{1}H, ^{2}H, and ^{3}He). The aim is to explore in greater detail the evolution of the damping in the transition from light to heavy nuclei.

The measurements were obtained with the Glasgow tagger [11] installed at the MAMI electron accelerator in Mainz, Germany [12]. The experimental approach is similar to that used by Armstrong *et al.* at Daresbury in 1972 [13,14] where hadronic products were measured in a detector of large angular acceptance.

With the present detector $\simeq$75% of the total cross sections can be measured directly. A discussion of the techniques developed to estimate the remaining 25% and their accuracy constitutes the major part of this paper.

II. EXPERIMENTAL SETUP

The tagged photon beam was produced by bremsstrahlung of the 855 MeV electrons from MAMI on a thin gold converter of 10^{-4} radiation lengths. The tagging system covers a photon energy range of 50–800 MeV with 352 counters, each having an energy resolution $\sim$2 MeV.

A. The photon beam

The photon flux was measured continuously with the aid of a detector placed in the beam downstream of DAPHNE. Incident photons were converted into e^+e^- pairs by a 5 mm copper converter and detected in coincidence in two plastic scintillator layers placed directly behind. The efficiency of

*Present address: GANIL, Bd. Henri Bequerel, 14000, CAEN, France.
†Permanent address: Faculté des Sciences, 5000 Monastir, Tunisia.
‡Permanent address: Department of Physical Sciences, Glasgow Caledonian University, Glasgow G4 OBA, United Kingdom.
§Electronic address: PEDRONI@PAVIA.INFN.IT

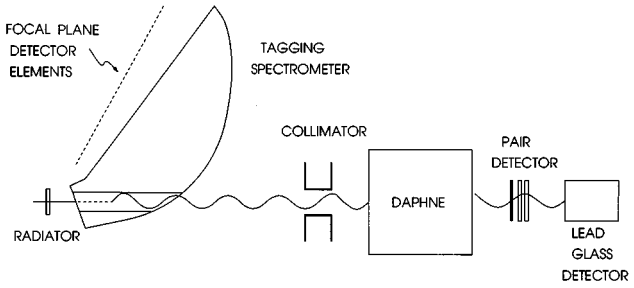

FIG. 1. Schematic view of the experimental layout.

this device was calibrated at low beam intensity against a lead-glass detector. The number of coincidences between the pair detector and each channel of the tagging system gave the number of tagged photons with a precision of the order of $\pm 2\%$. The general layout of the system is shown in Fig. 1.

B. The detector

A detailed description of the DAPHNE detector is given in Ref. [15]. The angular coverage runs from 21° to 159° in the polar direction and the complete 360° in the azimuthal direction. This corresponds to $\sim 94\%$ of 4π.

Three concentric multiwire proportional chambers (MWPC's) are used to reconstruct the charged particle trajectories, while three layers of scintillator placed around the MWPC's (A, B, and C in Fig. 2) enable particle identification [16]. The external photon converters (D, E, and F in Fig. 2), made up of lead-scintillator sandwiches, allow the detection of neutral pions.

Protons and $\pi^{\pm}$ detected in DAPHNE can be identified with the aid of a ''range method'' [16]. This method makes use of the known energy loss characteristics of the particles as a function of the distance traveled within the detector.

The π^0's are detected via their disintegration into photons. The detection efficiency for a single γ ray is of the order of 60%, but several conditions are imposed on the experimental events in order to completely eliminate all background: (i) only multiplicity two neutral events in non-adjacent detector sectors are considered; (ii) photons converted in the lead-scintillator sandwich are accepted only if a signal is detected in two consecutive layers of the same sector; (iii) for photons converted in the B layer, a software threshold is set on the energy deposited in this layer.

Due to these constraints, only a modest π^0 detection efficiency ($\sim 20\%$) is achieved but, as they mostly depend on the detector geometry, this efficiency is modeled accurately by simulation.

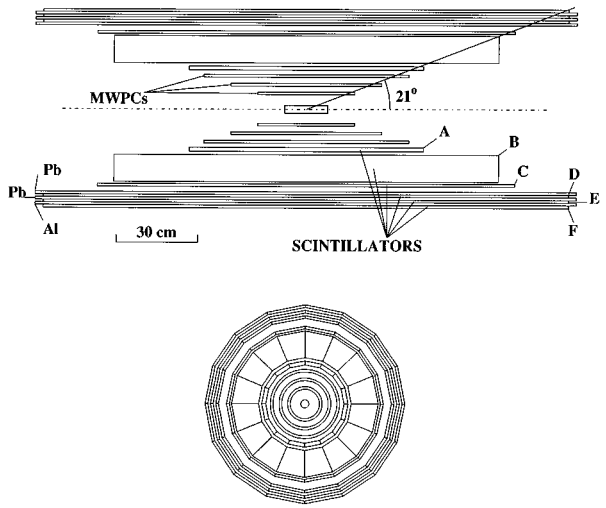

FIG. 2. Longitudinal (top) and transverse (bottom) views of the DAPHNE detector.

C. The target

The target cell is a cylinder 25 cm in length and 4.3 cm in diameter, the walls of which are made from 170 μm thick Mylar. This cell can be filled with liquid ^{1}H, ^{2}H, ^{3}He, or ^{4}He. The cooling system consists of two loops based on a Gifford-McMahon refrigerator which brings the ^{4}He coolant to 17 K, and is used to cool down ^{1}H and ^{2}H targets. To obtain lower temperatures, a Joule-Thomson valve is coupled to the high pressure of the Gifford-McMahon refrigerator and a temperature of 2.5 K is reached by pumping the ^{4}He bath after the Joule-Thomson valve.

The pressure and temperature may be remotely controlled with the aid of small heating resistors placed at various points in the loop. This results in a target stability of 1 mbar in pressure and 0.01 K in temperature, thus ensuring a target density stability of 0.5%.

III. DATA ANALYSIS

The general analysis procedure which has been developed to determine the total photoabsorption cross section is not based on the sum of all partial channels for photoproduction and photodisintegration. This would have been possible with the DAPHNE detector for the three light nuclei ^{1}H, ^{2}H, or ^{3}He where the final-state multiplicity is low. However, we have chosen a more global technique which limits the systematic errors and will be described in detail for the hydrogen case.

If we consider a hydrogen target and photon energies $E_\gamma < 450$ MeV, $\sigma_{\rm tot}$ comprises two contributing channels, $p\pi^0$ and $n\pi^+$. Taking into account DAPHNE's acceptance and the proton detection threshold of 300 MeV/c, about half of $\sigma(p\pi^0)$ can be accessed by measuring the proton and the remainder by detecting the π^0. This is possible since the π^0 detection efficiency ϵ_{π^0} is finite for all π^0 energies and angles. When the proton is not detected, the π^0 is used as the signature for $p\pi^0$. The situation is not so straightforward for $\sigma(n\pi^+)$. Since DAPHNE is not used to detect neutrons, a single π^+ is the required signature, and due to cuts on the angular and momentum distributions, only 90% of $\sigma(n\pi^+)$ can be measured directly. The procedures to estimate the missing 10% are described in Sec. III B.

To summarize, $\sigma_{\rm tot}$ can be expressed as a sum of three terms:

$$\sigma_{\rm tot} \propto N_{\rm ch} + N_{\pi^0} \cdot \frac{1}{\epsilon_{\pi^0}} + \Delta N_{\pi^+},$$

where $N_{\rm ch}$ is the number of charged events; N_{π^0} is the number of single measured π^0 events with no accompanying

charged particle; ϵ_{π^0} is the π^0 detection efficiency; and ΔN_{π^+} is the unmeasured charged pion contribution obtained by extrapolation.

The same technique can be applied at higher energies to multipion final states and the specific treatment will be described later. When this approach is extended to analyzing the deuterium and ^{3}He data, $\sigma_{\rm tot}$ can again be expressed as the sum of these three terms plus the additional photodisintegration terms.

Before discussing how ϵ_{π^0} and ΔN_{π^+} are evaluated, a comment on the electromagnetic background is appropriate. Since electromagnetic events are strongly forwardly peaked, only a very small fraction interact in DAPHNE. In the next section it will be shown that it is straightforward to suppress the electromagnetic background without affecting the nuclear events.

A. π^0 detection

All π^0 production channels on the proton and neutron are considered in the analysis. The single π^0 channels are

$$\text{(a)}\quad \gamma+p\rightarrow p+\pi^0,\quad \text{(a}')\quad \gamma+n\rightarrow n+\pi^0,$$
$$\text{(b)}\quad \gamma+p\rightarrow n+\pi^+ +\pi^0,\quad \text{(b}')\quad \gamma+n\rightarrow p+\pi^- +\pi^0.$$

For each of the reactions listed above, the efficiency for detecting a single π^0, ϵ_{π^0}, was determined using a GEANT simulation which takes into account the full geometrical complexity of the setup and the electronic thresholds. We have verified that changing the detector threshold values by $\pm 10\%$ corresponds to a relative change of $\pm 4\%$ in the detection efficiency. We take this value as the systematic error on ϵ_{π^0}. The corresponding maximum uncertainty in $\sigma_{\rm tot}$ is at $E_\gamma \simeq$ 250 MeV, where $N_{\pi^0}\epsilon_{\pi^0}^{-1}$ accounts for less than 50% of the total cross section as all recoil protons cannot be detected. This introduces a maximum uncertainty of $\pm 2\%$ on $\sigma_{\rm tot}$.

Process (a) was simulated using the published angular distributions [17]. Process (a′) was simulated in the same way, with the assumption that $d\sigma/d\Omega(p\pi^0)=d\sigma/d\Omega(n\pi^0)$. However, these two channels have slightly different ϵ_{π^0} values since occasionally a neutron can be misidentified as a γ ray. For processes (b) and (b′) the treatments of the three-body final states were undertaken using a three-body phase space distribution. The absolute values obtained varied typically between 20% and 23% for all four channels and consequently, for each target, an average ϵ_{π^0} value, $\bar{\epsilon}_{\pi^0}$, could be used. In determining the average efficiency the relative weighting for each channel was calculated by referring to the measured $(\pi^\pm\pi^0)$ and $(p\pi^0)$ coincidence event rates.

Processes involving double π^0 production are not given any special treatment in the final analysis. This is justified by considering their contribution at 700 MeV where they account for around 4% of $\sigma_{\rm tot}$ so that even the presence of a large error does not affect $\sigma_{\rm tot}$ significantly. In addition, at the upper limit of the energy range covered by the measurement, triple π^0 production occurs. This is dominated by η production which has a threshold at $\sim$ 710 MeV. Since the π^0 multiplicity cannot be determined in DAPHNE, there is a small uncertainty in estimating ϵ_{π^0} at very high energies. The effect of these approximations is to introduce a maximum overestimation of $\simeq 10$ μb in $\sigma_{\rm tot}$ for $E_\gamma >$ 700 MeV. This overestimation was taken into account when determining the experimental cross sections.

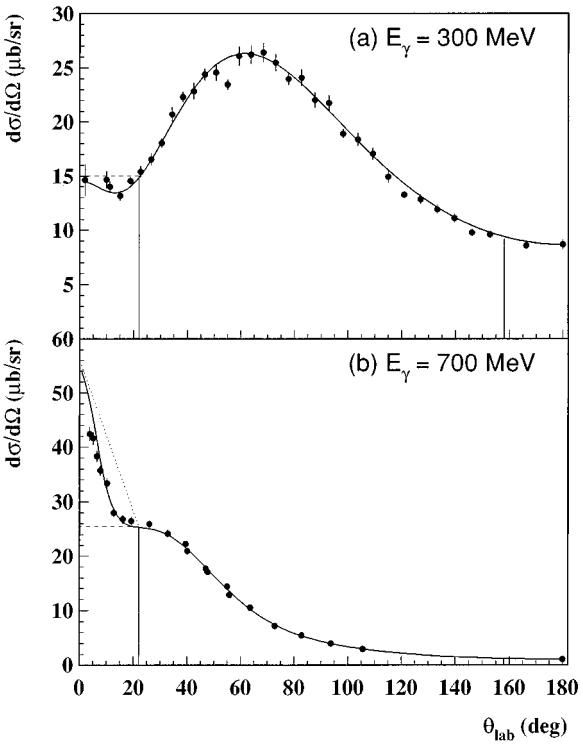

FIG. 3. Angular distribution $\gamma+p\rightarrow n+\pi^+$ at 300 MeV (a) and at 700 MeV (b) from Ref. [17]. The different line styles indicate the different extrapolations discussed in the text.

B. Extrapolation techniques

The third term in the expression for $\sigma_{\rm tot}$ is a correction for the unmeasured charged pion contribution and is obtained by angular and momentum extrapolations of the single charged pions spectra. Before this correction was evaluated we ensured that in the general analysis which identifies charged pions, no double counting has occurred when double pion photoproduction channels are involved. This can be illustrated by considering the $\gamma p\rightarrow p\pi^+\pi^-$ channel. Since π^+ and π^- cannot be distinguished in DAPHNE, the sum of singly detected charged pions is thus a mixture of the two. The event rate for either the π^+ or π^- is therefore half of the total. This double counting is evaluated from the $(\pi^\pm\pi^\mp)$ coincidence rate and subtracted from the single pion spectra. For the same reason, the charged pions from $\pi^\pm\pi^0$ channels are carefully accounted for from the measured $(\pi^\pm\pi^0)$ coincidence rate. These pions are subtracted from the spectra to be extrapolated as the corresponding channels have already been fully accounted for within the π^0 detection efficiency.

1. Angular extrapolations

These extrapolations were carried out to estimate the contributions from the polar angular ranges [0°,21°] and [159°,180°] which lie outside the DAPHNE geometrical acceptance. Figure 3 shows examples of the π^+ differential

cross sections for the reaction $\gamma p \rightarrow n\pi^+$ at $E_\gamma = 300$ and 700 MeV. The vertical lines show the angular range covered by DAPHNE and the solid line is a global best fit to the published data [17]. The data points are also from Ref. [17]. These two differential cross sections, $d\sigma/d\Omega$, represent extreme cases of the behavior at forward angles and highlight the region of greatest uncertainty.

To obtain the upper and the lower limits for the missing cross section, $d\sigma/d\Omega$ may be taken to be constant in the forward angles, as shown by the dashed line in Figs. 3(a) and 3(b), or linearly increasing for decreasing angles, as shown by the dotted line in Fig. 3(b). The estimations of the forward missing cross section, i.e., $2\pi\int_0^{21}(d\sigma/d\Omega)\sin\theta\, d\theta$, based on these two extrapolations differ at most by 33% in the extrapolated values. The average was chosen for the final extrapolation and a systematic error of $\pm 16\%$ on the extrapolated value was assumed. As an example, for the proton at $E_\gamma = 300$ MeV, the missing cross section is 3.1% of the total $n\pi^+$ cross section at forward dead angles and 1.7% at backward angles. This results in a $\pm 0.4\%$ systematic error in the $\sigma_{\rm tot}$ evaluation. The strongest contribution to the systematic error is at $E_\gamma = 700$ MeV where the missing cross section is 12% of the total $n\pi^+$ cross section and 4.9% of $\sigma_{\rm tot}$. This corresponds to a maximum systematic error of $\pm 0.8\%$ of $\sigma_{\rm tot}$.

2. Momentum extrapolations

The charged pion momentum distributions were reconstructed by using the ''range method'' [16] for events that stopped within the detector. For single pion photoproduction the two-body kinematics imposes limits on both the upper and lower momenta of the pions. However, for $E_\gamma > 200$ MeV, the lower momentum limit is above the detection threshold limit of DAPHNE and hence no extrapolation below the threshold is required. The three-body kinematics of double pion production however, has a lower pion momentum limit of zero. In this case a linear extrapolation to zero is used since the corresponding correction is less than 1% of $\sigma_{\rm tot}$.

C. Electromagnetic shower contribution

Cuts were imposed on the charged particle energy losses in order to eliminate most of the electrons.

The effect of the remaining electron contamination is seen in the pion angular distributions. The magnitude of the effect decreases with increasing photon energy as the associated background becomes increasingly forwardly peaked. In Figs. 4–6 the ''pion'' differential cross sections at 140 MeV, 215 MeV, and 371 MeV, respectively, are presented as a function of $\theta_{\rm c.m.}$. The events shown in Fig. 4, being below pion detection threshold, are purely electromagnetic in origin, and give an estimation of the maximum magnitude of the background. The forward peak in Fig. 5 is due to a mixture of electrons and pions. Comparing this with the published pion angular distributions of Ref. [17] (shown as a solid line) allows the electron background to be evaluated. This correction to the cross section is small, being at most 4 μb at 200 MeV and falls to zero by 370 MeV as seen in Fig. 6. Consequently it does not significantly contribute to the systematic error.

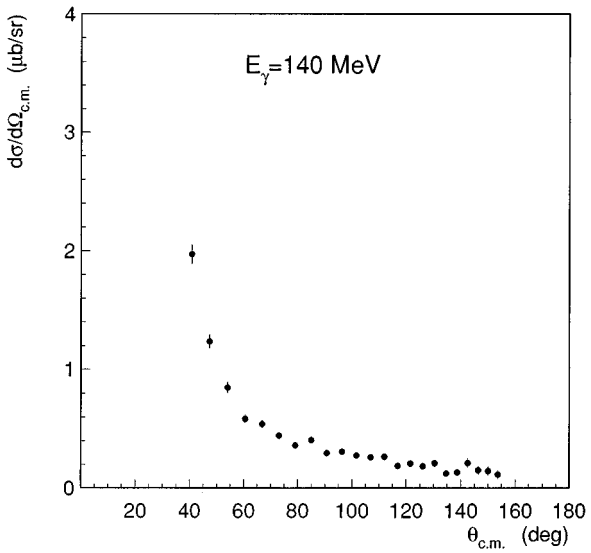

FIG. 4. Electrons initially identified as π^+ and put through the kinematics for the process $\gamma + p \rightarrow n + \pi^+$.

The electromagnetic background contamination can therefore be removed effectively without resorting to the use of forward veto detectors. This gives DAPHNE a significant advantage over other detector systems which rely on such detectors [13,14] which are invariably susceptible to hadronic interactions.

D. Corrections

In order to avoid any edge effects which could affect the detection efficiency, and as the polar and azimuthal angles are measured with a high precision, cuts in θ and ϕ are applied in the analysis. These cuts reduce the azimuthal acceptance to 84% of 2π and the polar acceptance to between 21° and 159°. Furthermore, in order to ensure that neither exit nor entrance windows contribute to the charged particle

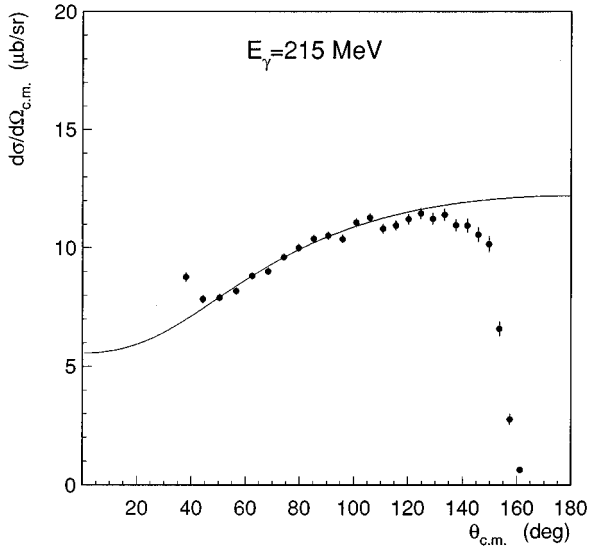

FIG. 5. Differential cross section $\gamma + p \rightarrow n + \pi^+$ at 215 MeV as a function of $\theta_{\rm c.m.}$. The solid curve is from Ref. [17]. The forward peak is contaminated by electrons.

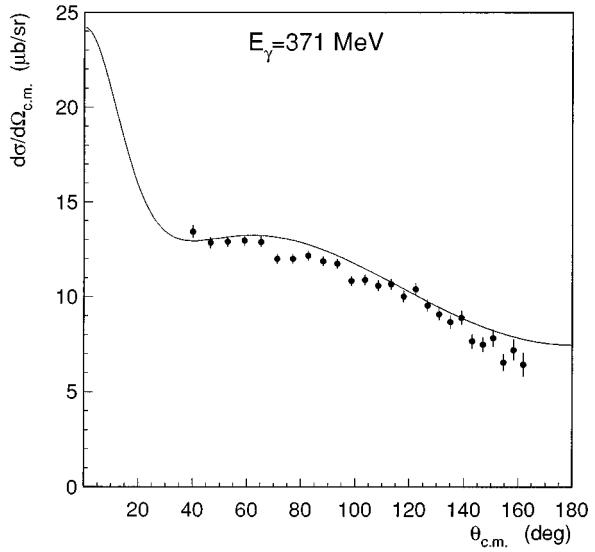

FIG. 6. Differential cross section $\gamma+p\rightarrow n+\pi^+$ at 371 MeV as a function of $\theta_{\text{c.m.}}$. The solid curve is from Ref. [17]. There is no evidence of electron contamination.

spectra, only events originating in a central target volume, corresponding to 15 cm of the full 25 cm length, are accepted. This finite target length and the measured beam profile (spot size of 20 mm in diameter) are taken into account in a Monte Carlo calculation of the solid angle which evaluates the angular acceptance as a function of the polar angle. These geometrical cuts have three consequences.

(1) The overall geometry is perfectly determined. The angular acceptance can be easily calculated without any ambiguity and the trajectory reconstruction efficiency is found to be uniform at $98.5\pm1\%$. This efficiency is determined experimentally by using both cosmic-ray events and photoreaction data. An important part of the events arising from $\gamma p\rightarrow p\pi^0$, $\gamma n\rightarrow n\pi^+$, and $\gamma p\rightarrow p\pi^+\pi^-$ can be discriminated by only using scintillator signals. The trajectory reconstruction efficiency is then determined by measuring the fraction of events that have both unambiguous signals in the scintillators and a reconstructed trajectory from the wire chambers.

(2) The cuts in the polar acceptance increase the angular extrapolation and consequently the systematic error is larger and taken as $\pm16\%$ as previously described in Sec. III B 1.

(3) The cuts in the azimuthal angle and the finite length of the target induce a correction which has to be applied only to the raw number of single pions. This correction is perfectly calculable but the determination of the pion spectra, to which it has to be applied, introduces a systematic error which will be discussed in Sec. IV B.

Losses due to hadronic interactions of charged pions in the target and the wire chambers must be accounted for. Below 400 MeV, only the $n\pi^+$ channel contributes to these spectra while above this value there is the additional $p\pi^+\pi^-$ contribution (see Sec. III B). However, if one takes the relative counting rates for these channels one discovers that only $\simeq10\%$ of $p\pi^+\pi^-$ events show up in the single pion spectra and consequently, above 400 MeV, at least 90% of single pions come from $n\pi^+$ events. For this last reaction we use a modified GEANT code which includes the hadronic cross sections for the target and wire chamber materials along with the published angular distributions for $\gamma p\rightarrow n\pi^+$ (Ref. [17]). The correction varies as a function of photon energy from a maximum of 5% of the $\gamma p\rightarrow n\pi^+$ cross section at $E_\gamma=300$ MeV to a value $\leqslant 1\%$ for $E_\gamma\leqslant300$ MeV. This corresponds to a maximum correction of 2.4% to σ_{tot} at $E_\gamma=300$ MeV. In view of the magnitude of this correction and the relative contribution of the single and double pion production channels to the single pion spectra, it is not considered necessary to correct for the double pion production case.

The raw single charged pion spectra are corrected for all of the above effects before the extrapolations are carried out.

Since the origin of π^0 events is unknown an empty target contribution of 1% is subtracted. This quantity is measured in dedicated ''empty target'' runs.

IV. THE HYDROGEN CROSS SECTION

The main advantage of the present method is that the total cross-section evaluation only requires particle identification for the extrapolations. However, without requiring additional analysis, the single pion photoproduction channels on the proton can also be evaluated in a restricted energy range and checked against previous data.

The cross section on hydrogen from 200 MeV to $\sim$400 MeV may be written as the sum of the two partial channels:

$$\sigma_{\text{tot}}(p\pi^0)=C\{N_p+N_{\pi^0}\epsilon_{\pi^0}^{-1}\}$$

and

$$\sigma_{\text{tot}}(n\pi^+)=C\{N_{\pi^+}+\Delta N_{\pi^+}\},$$

where

$$C=\frac{1}{N_\gamma N_T}$$

and N_p is the total number of protons detected; N_{π^+} is the measured π^+ contribution; ΔN_{π^+} is the sum of all the corrections and extrapolations for charged pions; N_{π^0} is the total number of unaccompanied π^0's detected; ϵ_{π^0} is the π^0 detection efficiency for the $p\pi^0$ channel; N_γ is the total number of photons, and N_T is the total number of target atoms.

Figures 7(a) and 7(b) show the results obtained for these two partial channels compared to previously published data [17]. The agreement is very good and indicates that the π^+ and p discrimination is excellent and the π^0 detection efficiency is well determined.

A. The total cross section

As outlined in Sec. III the total photoabsorption cross section for hydrogen from 200 to 800 MeV may be written as

$$\sigma_{\text{tot}}=C\{N_{\text{ch}}+\Delta N_{\pi^\pm}+N_{\pi^0}(\bar{\epsilon}_{\pi^0})^{-1}\},$$

where N_{ch} is the total number of events having at least one charged particle and $\Delta N_{\pi^\pm}$ is the total unmeasured charged pion contribution.

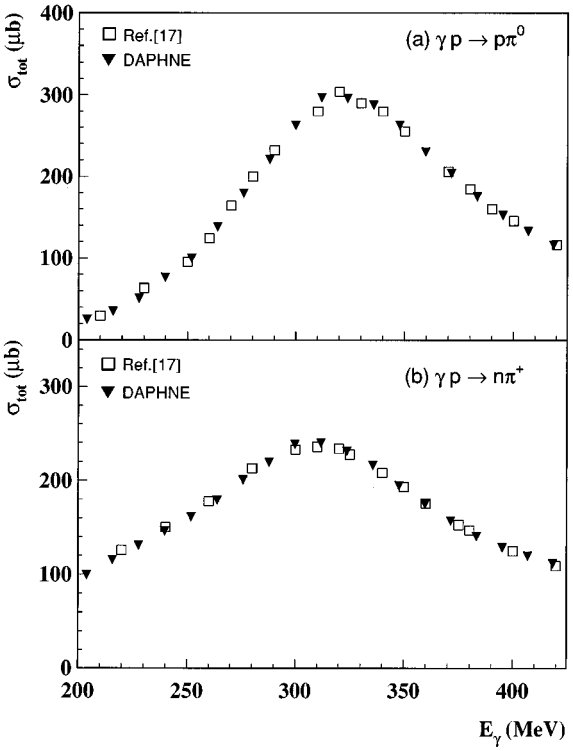

FIG. 7. Total cross section $\gamma+p\rightarrow p+\pi^0$ (a) and $\gamma+p\rightarrow n+\pi^+$ (b) from 200 MeV to 425 MeV for the present measure compared to the data from Ref. [17]. Statistical errors are included but are smaller than the symbols' size.

For the proton at $E_\gamma = 300$ MeV, $N_{\rm ch}$ accounts for 72% of $\sigma_{\rm tot}$ and N_{π^0} makes up a further 5%. The correction for the π^0 detection efficiency brings in 20% of the missing 23% and ΔN_{π^+} accounts for the remaining 3%.

We point out that charged particle discrimination is needed only in the evaluation of the ΔN_{π^+} term, which gives a maximum contribution of 6% to $\sigma_{\rm tot}$ at E_γ=700 MeV, and it is not required for $N_{\rm ch}$ that corresponds to the total number of hadronic charged events independently of their nature and represents 60% of the total cross section at E_γ=250 MeV and 79% at E_γ=700 MeV.

B. Systematic errors

We recall the systematic error contributions with respect to $\sigma_{\rm tot}$: target density = $\pm 0.5\%$; number of photons = $\pm 2\%$; angular extrapolations $\leqslant \pm 1\%$; and π^0 efficiency $\leqslant \pm 2\%$. The correction for the target length and the cut in ϕ, which is about 25%, introduces a last source of systematic error coming from the evaluation of the raw number of single charged pions to which this correction is applied. Let us consider this in more detail. At low photon energy there are only two channels, $n\pi^+$ and $p\pi^0$. For $E_\gamma \leqslant$ 260 MeV on hydrogen no proton is detected, all charged events are pions, i.e., $N_{\rm ch} = N_{\pi^+}$. The only error comes from the trajectory reconstruction efficiency, namely, 1% of $N_{\rm ch}$. At higher energies there are five channels:

$$\text{(a) } n\pi^+, \quad \text{(b) } p\pi^0, \quad \text{(c) } p\pi^+\pi^-,$$
$$\text{(d) } n\pi^+\pi^0 \quad \text{(e) } p\pi^0\pi^0.$$

As previously described, there is no correction for channels (b), (d), and (e) which involve a π^0. The correction should then be applied to the pions coming from (a): $N_{\pi^+}(n\pi^+)$ plus half the number of pions coming from (c): $1/2N_{\pi^\pm}(p\pi^+\pi^-)$. At 699 MeV these two contributions correspond to 73 μb, i.e., $\sim$1/4 of $\sigma_{\rm tot}$. The determination of this number depends on (i) the $p-\pi^\pm$ discrimination. As shown in [16] the misidentification due to the nuclear interactions of the protons are small; (ii) the trajectory reconstruction efficiency (98.5%); (iii) the substraction of the pions from (d) and half the pions coming from (c). These two quantities are evaluated from the $(\pi^\pm\pi^\mp)$ and $(\pi^+\pi^0)$ coincidence rates.

Assuming an error of 10% in the determination of the number of pions to be extrapolated, the systematic error is then (73 μb $\times$ 0.25 $\times$ 0.1) = 1.83 μb. Adding in quadrature the contribution due to the trajectory reconstruction efficiency (73 μb $\times$ 0.01 = 0.73 μb), we get a total systematic error of 2 μb. This is, as in the low energy case, equal to 1% of the total number of charged events $N_{\rm ch}$ (218 μb). In practice, over all the energy range a systematic error of 1% of $N_{\rm ch}$ is assumed.

Table I summarizes for two energies the systematic errors and gives the total combined systematic error obtained by summing in quadrature the different contributions. The first two errors do not vary with incident energy. However, the latter two have a strong variation with energy, the effect of which can be seen in this table.

Surprisingly, we see that the dominant contribution comes from the determination of the photon number and not from the different extrapolations.

V. $\sigma_{\rm tot}$ ON ^{2}H AND ^{3}He

For these total cross sections the pion photoproduction channels are evaluated from the experimental data using the procedures developed in the hydrogen analysis. In addition,

TABLE I. The different contributions (in μb) to the total systematic error are shown at E_γ=252 MeV and E_γ=699 MeV. See the text for explanation of the different symbols. At E_γ=252 (700) MeV, the contributions of $N_{\rm ch}$, N_{π^0}, and $\Delta N_{\pi^\pm}$ to $\sigma_{\rm tot}$ are 152 (218) μb, 100 (30) μb, and 8 (14) μb, respectively.

E_γ (MeV)	$\sigma_{\rm tot}$ (μb)	$\Delta_{\rm sys}(N_\gamma)$	$\Delta_{\rm sys}$ (target density)	$\Delta_{\rm sys}(N_{\rm ch})$	$\Delta_{\rm sys}(\epsilon_{\pi^0})$	$\Delta_{\rm sys}(\Delta N_{\pi^\pm})$	Total (sum in quadrature)
252	260	5.2	1.3	1.5	4	1.3	7 μb
699	262	5.2	1.3	2.2	1.2	2.2	7 μb

since the main contribution to π^0 production is from quasi-free processes, the π^0 treatment does not differ significantly from the case for hydrogen. However, a more comprehensive treatment of the photodisintegration channels is required for these nuclei.

A. Photodisintegration processes

1. $\gamma + {}^2H \rightarrow p + n$

Most of the photodisintegration of the deuteron is measured within the detector's acceptance. However, protons falling either outside the angular acceptance or below the detection threshold must be taken into account. The two-body break-up channel has been studied in detail with DAPHNE and analyzed as part of an independent study [18]. The results from [18] are used to estimate the missing contribution $\Delta pn(^2\mathrm{H})$ for the present case. The maximum correction occurs around $E_\gamma = 300$ MeV and is $\sim$ 0.5% of σ_{tot}.

2. $\gamma + {}^3He \rightarrow p + n + p_{spectator}$

The missing contribution $\Delta pn(^3\mathrm{He})$ of this reaction is taken to be

$$\Delta pn(^3\mathrm{He}) = \Delta pn(^2\mathrm{H}) \cdot \alpha.$$

The parameter

$$\alpha = \frac{\gamma + {}^3\mathrm{He} \rightarrow p + n + p_{\mathrm{spectator}}}{\gamma + {}^2\mathrm{H} \rightarrow p + n}$$

has been previously evaluated up to 340 MeV and is found to be approximately constant for all photon energies with a value of 1.68 [19]. We assume that this constant is valid up to 790 MeV. This correction accounts for 0.5% of σ_{tot} at 300 MeV and contributes, at maximum, for 0.2% of σ_{tot} above 400 MeV. Consequently, a large systematic error due to the assumption made does not significantly contribute to the systematic error of σ_{tot}.

3. $\gamma + {}^3He \rightarrow p + p + n$ and $\gamma + {}^3He \rightarrow p + d$

A study of these photodisintegration channels has been made with DAPHNE [20,21]. These analyses provide the missing ppn contribution Δppn for the present experiment and show that the losses in the pd channel are negligible. The correction Δppn is calculated assuming a three-body phase space distribution and has an effect of less than 0.3% on the ^{3}He total cross section.

B. Coherent π^0 production

The channels $\gamma + {}^2\mathrm{H} \rightarrow {}^2\mathrm{H} + \pi^0$ and $\gamma + {}^3\mathrm{He} \rightarrow {}^3\mathrm{He} + \pi^0$ have not been given special consideration. It is estimated that ϵ_{π^0} in this case is similar to that for the $p\pi^0$ channel and the systematic error introduced is less than the overall systematic error of $\pm 2\%$ in π^0 efficiencies.

C. Cross-section calculations for ^{2}H and ^{3}He

The final calculations of σ_{tot} for deuterium and ^{3}He are written as

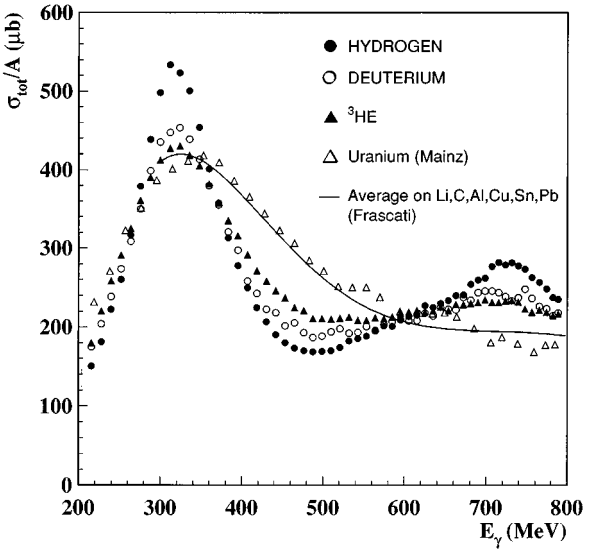

FIG. 8. The total photoabsorption cross sections per nucleon from 200 MeV to 800 MeV for ^{1}H (solid circles), ^{2}H (open circles), and ^{3}He (solid triangles) are compared to the average for heavier nuclei (curve) [7] and to the result for U (averaged on ^{235}U and ^{238}U) [8] (open triangles). Statistical errors are included but are smaller than the symbols' size.

$$\sigma_{\mathrm{tot}}(^2\mathrm{H}) = C\{N_{\mathrm{ch}} + \Delta N_{\pi^\pm} + N_{\pi^0}(\bar{\epsilon}_{\pi^0})^{-1}\} + \Delta pn(^2\mathrm{H}),$$

$$\sigma_{\mathrm{tot}}(^3\mathrm{He}) = C\{N_{\mathrm{ch}} + \Delta N_{\pi^\pm} + N_{\pi^0}(\bar{\epsilon}_{\pi^0})^{-1}\} + \Delta pn(^3\mathrm{He}) + \Delta ppn(^3\mathrm{He}).$$

VI. RESULTS AND COMMENTS

Figure 8 shows σ_{tot}/A for the ^{1}H, ^{2}H, and ^{3}He along with the Mainz result on U [8] and the average result obtained at Frascati for medium and heavy nuclei [7]. Table II lists the final absolute cross-section values and the associated experimental errors as a function of photon energy.

As is shown in Figs. 9 and 10, except for a slight difference at $E\gamma \simeq$ 260 MeV and in the valley between the resonances at $E\gamma \simeq$ 450 MeV, the results for ^{1}H and ^{2}H are in good agreement with the older Daresbury data [13,14]. Also shown in Fig. 9 is the sum of $p\pi^0$ and $n\pi^+$ channels ([17]) below $E\gamma \simeq$ 450. These are effectively the only reactions involved for hydrogen in this energy region.

In comparing the three nuclei (^{1}H, ^{2}H, and ^{3}He) it is seen that σ_{tot}/A in the Δ resonance region is reduced in amplitude and increased in width in proceeding from ^{1}H to ^{3}He. This effect was investigated by Carrasco and Oset [22] in the framework of a many-body theory. They considered the effects of the inter-nucleon medium on this resonance and succeeded in reproducing the behavior of σ_{tot}/A observed in the heavier nuclei.

Although the D_{13} resonance is strongly damped for ^{3}He it can still be observed, which is not the case for heavier nuclei where there is no evidence of the resonance in σ_{tot}.

In an attempt to explain this ''damping'' effect several models have been proposed [23–26], each taking a different approach to the problem. Precise calculations with these models can be carried out as the wave functions for the light

TABLE II. The total photoabsorption cross sections (in μb) for ^{1}H, ^{2}H, and ^{3}He determined for 70 photon energy bins centered on the specified value of E_γ. Both statistical ($\pm\Delta\sigma_{\rm stat}$) and systematic errors ($\pm\Delta\sigma_{\rm sys}$) are given. The latter were calculated by adding in quadrature the different contributions listed in Sec. IV.

	^{1}H			^{2}H			^{3}He		
E_γ (MeV)	$\sigma_{\rm tot}$ (μb)	$\Delta\sigma_{\rm stat}$ (μb)	$\Delta\sigma_{\rm sys}$ (μb)	$\sigma_{\rm tot}$ (μb)	$\Delta\sigma_{\rm stat}$ (μb)	$\Delta\sigma_{\rm sys}$ (μb)	$\sigma_{\rm tot}$ (μb)	$\Delta\sigma_{\rm stat}$ (μb)	$\Delta\sigma_{\rm sys}$ (μb)
204	125	1	3	282	3	7	435	2	11
216	150	1	4	350	3	9	540	2	14
228	181	1	5	409	4	10	661	3	19
240	223	1	6	477	4	14	774	3	22
252	260	1	7	547	4	16	872	4	26
264	317	1	10	617	5	18	975	4	29
276	379	1	11	700	5	21	1083	4	32
288	438	1	13	798	6	24	1171	4	35
300	498	1	15	870	6	27	1238	4	36
312	534	1	15	894	6	28	1281	5	37
324	523	1	14	906	6	28	1290	5	37
336	500	1	14	878	6	28	1255	5	35
348	453	1	12	827	6	25	1216	5	33
360	401	1	11	759	6	23	1146	5	31
371	358	1	9	710	6	22	1074	5	29
383	313	1	8	641	6	19	1005	5	27
395	278	1	7	595	6	17	947	5	25
407	250	1	7	516	5	17	875	5	23
419	225	1	6	485	5	14	814	4	21
430	207	1	5	445	7	13	774	4	20
442	190	1	5	437	5	13	738	4	19
453	180	1	4	403	5	11	712	4	18
465	174	1	4	411	5	11	674	4	17
476	170	1	4	386	5	10	663	4	17
488	169	1	4	374	5	10	633	4	18
499	169	1	4	377	5	10	633	5	16
510	170	1	4	388	5	10	630	5	15
521	174	1	4	396	5	11	635	5	16
532	183	1	4	385	5	10	639	5	16
543	186	1	4	387	5	10	627	5	15
554	189	1	4	402	6	11	626	5	15
564	196	1	5	391	6	8	635	5	16
575	202	1	5	407	6	10	633	5	16
585	201	1	5	415	6	11	640	5	16
595	211	1	5	419	6	11	654	5	17
605	214	1	5	416	6	11	658	6	17
615	215	1	5	417	6	10	664	6	16
625	227	1	6	436	6	11	658	6	16
635	225	1	6	429	6	11	663	6	17
644	230	1	6	451	7	11	676	6	17
654	234	2	6	446	7	11	663	6	16
663	240	1	7	444	7	11	688	6	17
672	241	1	7	476	7	12	687	6	17
681	254	2	7	468	7	12	691	6	17
690	260	2	7	488	7	12	693	6	18
699	262	2	7	491	7	13	705	6	18
707	277	2	7	491	7	12	695	6	17
715	282	2	8	487	8	12	694	7	18
724	279	2	8	477	8	12	700	7	18
732	282	2	8	467	8	12	701	7	18
739	278	2	8	475	8	12	695	7	18
748	273	2	8	496	8	13	669	6	17
756	263	2	7	473	8	13	657	6	17
765	257	2	7	453	7	12	665	6	17
774	248	2	7	447	8	12	657	6	17
782	238	2	6	430	8	12	644	7	16
789	235	2	6	437	9	13	651	8	16

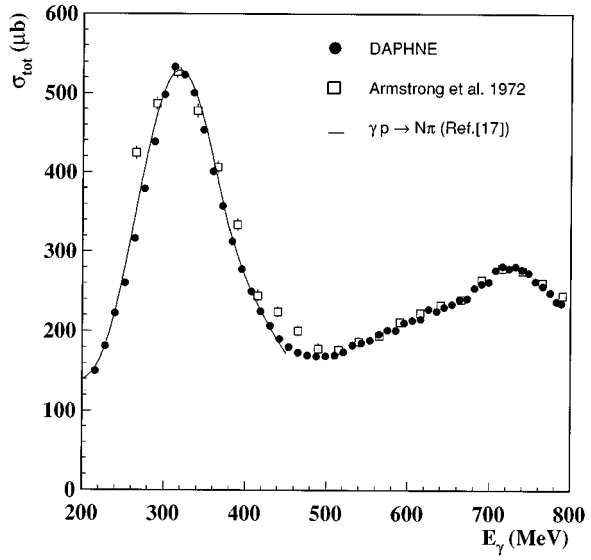

FIG. 9. The total cross section, $\sigma_{\rm tot}$, for hydrogen from 200 MeV to 800 MeV. The result obtained with DAPHNE is (solid circles) compared to that previously published by Armstrong *et al.* [13] (empty squares) and, below 450 MeV, with the sum of $\gamma+p\rightarrow n+\pi^+$ and $\gamma+p\rightarrow p+\pi^0$ channels (continuous line) [17].

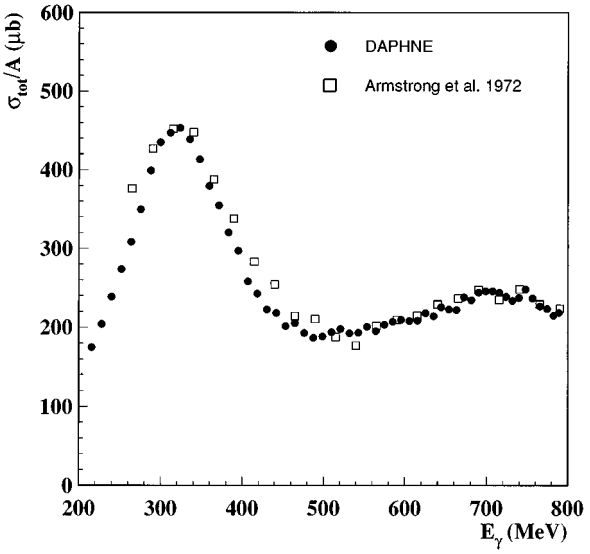

FIG. 10. The total cross section per nucleon, $\sigma_{\rm tot}/A$, for deuterium from 200 MeV to 800 MeV. The results obtained with DAPHNE (solid circles) are compared to those previously published by Armstrong *et al.* [14] (empty squares).

nuclei are well known and a comparison with the new data from the present measurements will make it easier to differentiate between the models.

VII. CONCLUSIONS

The total photoabsorption cross sections on ^{1}H, ^{2}H, and ^{3}He have been measured over the photon energy range 200–800 MeV. Thanks to the large detector acceptance and the excellent quality of the tagged photon beam, high precision measurements with small systematic errors were obtained.

The new ^{3}He measurement shows that this nucleus is an intermediate case between deuterium and heavy nuclei. It will therefore provide a strong constraint on the theories that are presently under development to explain the ''damping'' of higher resonances in heavier nuclei.

In order to complete this experimental study the ^{4}He total cross section has been measured with DAPHNE. The final results will be published in the near future.

[1] J. Ahrens, Nucl. Phys. **A446**, 229c (1985).
[2] R. Bergère, in *Proceedings of the 2nd Workshop on Perspectives in Nuclear Physics at Intermediate Energies*, Trieste, 1985, edited by S. Boffi, C. Ciofi degli Atti, and M.M. Giannini (World Scientific, Singapore, 1985), p. 153.
[3] P. Carlos, in *Proceedings of the International School of Intermediate Energy Nuclear Physics*, Verona, 1985, edited by R. Bergere, S. Costa, and C. Schaerf (World Scientific, Singapore, 1985), p. 1.
[4] N. Bianchi *et al.*, Phys. Lett. B **299**, 219 (1993).
[5] N. Bianchi *et al.*, Phys. Lett. B **309**, 5 (1993).
[6] M. Anghinolfi *et al.*, Phys. Rev. C **47**, R922 (1993).
[7] N. Bianchi *et al.*, Phys. Lett. **325**, 333 (1994).
[8] Th. Frommhold, F. Steiper, W. Henkel, and U. Kneissl, Phys. Lett. B **295**, 28 (1992); Th. Frommhold *et al.*, Z. Phys. A **350**, 249 (1994).
[9] A.K. Ananikyan *et al.*, Sov. J. Nucl. Phys. **46**, 208 (1987).
[10] E.A. Arakelyan *et al.*, Sov. J. Nucl. Phys. **38**, 589 (1983).
[11] I. Anthony, J.D. Kellie, S.J. Hall, G.J. Miller, and J. Ahrens, Nucl. Instrum. Methods Phys. Res. Sect. A **301**, 103 (1991).
[12] H. Herminghaus, A. Feder, K.H Kaiser, W. Manz, and H. v.d. Schmitt, Nucl. Instrum. Methods A **138**, 1 (1976).
[13] T.A. Armstrong *et al.*, Phys. Rev. D **5**, 1640 (1972).
[14] T.A. Armstrong *et al.*, Nucl. Phys. **B41**, 445 (1972).
[15] G. Audit *et al.*, Nucl. Instrum. Methods Phys. Res. Sect. A **301** 473 (1991).
[16] A. Braghieri *et al.*, Nucl. Instrum. Methods Phys. Res. Sect. A **343**, 623 (1994).
[17] H. Genzel, P. Joos, and W. Pfeil, in *Photoproduction of Elementary Particles*, edited by H. Schopper, Landolt-Börnstein, New Series, Group 1-Vol. 8 (Springer-Verlag, Berlin, 1973).
[18] R. Crawford, Ph.D. thesis, University of Glasgow, 1994.
[19] N. d'Hose *et al.*, Phys. Rev. Lett. **63**, 856 (1989).
[20] G. Audit *et al.*, to be submitted to Nucl. Phys.
[21] V. Isbert *et al.*, Nucl. Phys. **A578**, 525 (1994).
[22] R.C. Carrasco and E. Oset, Nucl. Phys. **A536**, 445 (1992).
[23] M.M. Giannini and E. Santopinto, Phys. Rev. C **49**, R1258 (1994).
[24] W.M. Alberico, G. Gervino, and A. Lavagno, Phys. Lett. B **321**, 177 (1994).
[25] S.V. Akulinichev and A.I. L'vov, Mainz Internal Report MKPH-T-93-1, 1993 (unpublished).
[26] L.A. Kondratyuk, M.I. Krivoruchenko, N. Bianchi, E. De Sanctis, and V. Muccifora, Nucl. Phys. **A579**, 453 (1994).